Inorganic Chemistry

pubs.acs.org/IC

Forum Article

796 nm Activation of a Photocleavable Ruthenium(II) Complex Conjugated to an Upconverting Nanoparticle through Two Phosphonate Groups

Michael S. Meijer, Marta M. Natile,* and Sylvestre Bonnet*

Cite This: *Inorg. Chem.* 2020, 59, 14807−14818

Read Online

ACCESS | Metrics & More | Article Recommendations | Supporting Information

ABSTRACT: The biological application of photoactivatable ruthenium anticancer prodrugs is limited by the need to use poorly penetrating high-energy visible light for their activation. Upconverting nanoparticles (UCNPs), which produce high-energy light under near-infrared (NIR) excitation, can solve this issue, provided that they form stable, water (H_2O)-dispersible nanoconjugates with the prodrug and that there is efficient energy transfer from the UCNP to the ruthenium complex. Herein, we report on the synthesis and photochemistry of the ruthenium(II) polypyridyl complex $[Ru(bpy)_2(\mathbf{3_H})](PF_6)_2$ ($[\mathbf{1}](PF_6)_2$), where bpy = 2,2-bipyridine and $\mathbf{3_H}$ is a photocleavable bis(thioether) ligand modified with two phosphonate moieties. This ligand was coordinated to the ruthenium center through its thioether groups and could be dissociated under blue-light irradiation. Complex $[\mathbf{1}](PF_6)_2$ was bound to the surface of $NaYF_4$:Yb^{3+},Tm^{3+}@$NaYF_4$:Nd^{3+}@$NaYF_4$ core−shell−shell (CSS-)UCNPs through its bis(phosphonate) group, thereby creating a H_2O-dispersible, thermally stable nanoconjugate (CSS-UCNP@[**1**]). Conjugation to the nanoparticle surface was found to be most efficient in neutral to slightly basic conditions, resulting in up to 2.4×10^3 Ru^{II} ions per UCNP. The incorporation of a neodymium-doped shell layer allowed for the generation of blue light using low-energy, deep-penetrating light (796 nm). This wavelength prevents the undesired heating seen with conventional UCNPs activated at 980 nm. Irradiation of CSS-UCNP@[**1**] with NIR light led to activation of the ruthenium complex $[\mathbf{1}](PF_6)_2$. Although only one of the two thioether groups was dissociated under irradiation at 50 $W \cdot cm^{-2}$, we provide the first demonstration of the photoactivation of a ruthenium thioether complex using 796 nm irradiation of a H_2O-dispersible nanoconjugate.

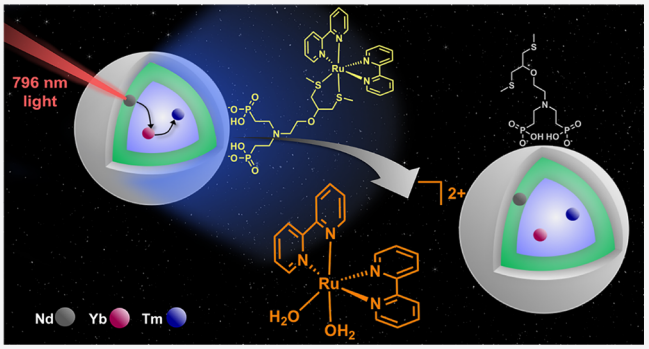

INTRODUCTION

In recent years, the use of light in the treatment of cancer has attracted significant attention.[1−3] Light can serve as a trigger for the activation of anticancer prodrugs. It provides both spatial and temporal control over drug activation and thus has the potential to improve the selectivity of chemotherapeutic agents. Ruthenium(II) polypyridyl complexes are among the compounds that have proven to be especially suitable for use in both classical photodynamic therapy (PDT) and photoactivated chemotherapy (PACT).[4−10] Whereas PDT relies on the generation of reactive oxygen species to kill cancer cells, PACT is independent of the presence of dioxygen and instead proceeds via the photodissociation of one of the ligands from the ruthenium center to induce cytotoxic effects. This dioxygen-independent mechanism makes PACT especially suitable for use in cases where PDT is less effective, e.g., in hypoxic tumors.[10] Unfortunately, most ruthenium polypyridyl complexes require high-energy visible light (400−500 nm) for their photoactivation, which both is harmful to cells[11] and penetrates human tissue poorly.[12] Ideally, one would use light in the "phototherapeutic window" (600−1000 nm) to activate such drugs. This can be achieved either by inducing a bathochromic shift in the singlet metal-to-ligand charge-transfer (^{1}MLCT) absorption bands of the ruthenium complex[10,13,14] or by using upconversion to generate the desired blue light locally, i.e., inside the tumor, from red light, as demonstrated recently by our group, among others, using triplet−triplet annihilation upconversion in liposomes.[15,16]

Lanthanoid-doped upconverting nanoparticles (UCNPs) are another promising system for upconversion-based PACT,[17] especially because they absorb near-infrared (NIR) light, are insensitive to the presence of molecular oxygen, are chemically stable, and show no photobleaching or photoblinking.[18]

Special Issue: Light-Controlled Reactivity of Metal Complexes

Received: January 6, 2020
Published: March 13, 2020

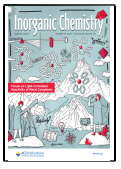

https://dx.doi.org/10.1021/acs.inorgchem.0c00043
Inorg. Chem. 2020, 59, 14807−14818

Scheme 1. Schematic Impression of the Synthesized Nanoparticle System CSS-UCNP@[1] and Its Method of Photoactivation

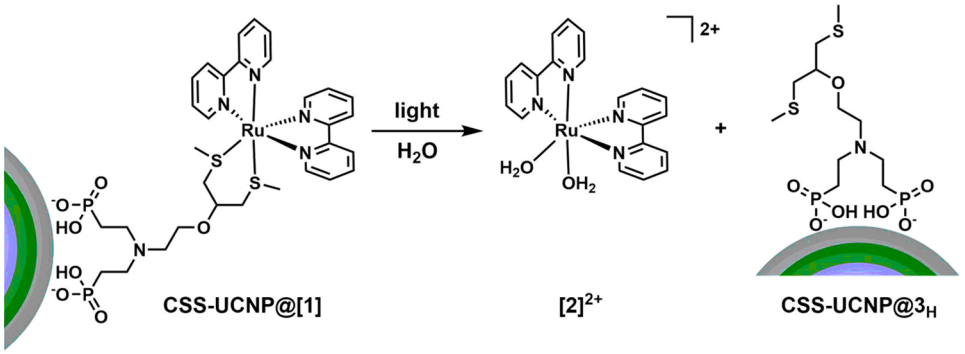

Typically consisting of a $NaYF_4$ host lattice doped with Yb^{3+} ions and either Tm^{3+} or Er^{3+} ions, UCNPs are able to produce blue, green, and red light under NIR irradiation.[19] Over the last 2 decades, UCNPs have been used for a wide range of applications, such as in bioimaging and biosensing,[20,21] drug delivery,[22] phototherapy,[23−25] optical thermometry,[26−28] photocatalysis,[29,30] photovoltaics,[31] or security.[32] The multicolor emission obtained with thulium-doped UCNPs allows for the simultaneous performance of therapy using the 450 nm emission and imaging using the 800 nm emission band in so-called theranostic applications.[33]

Typically, the excitation of UCNPs is performed near 980 nm, which matches the main absorption peak ($^2F_{7/2} \rightarrow {}^2F_{5/2}$) in Yb^{3+}. Unfortunately, because of the presence of a water (H_2O) absorption peak at 980 nm, prolonged irradiation of aqueous samples using high-intensity light of this wavelength leads to strong heating effects, potentially harmful in biological applications.[34] By codoping the host lattice with Nd^{3+} ions, the excitation wavelength can be shifted to 800 nm, avoiding these undesired heating effects.[35,36] However, energetic resonance between some of the 4f−4f transitions in Tm^{3+} and Nd^{3+} can lead to deleterious cross-relaxation, and a dramatic reduction in the upconversion quantum yield, when these two lanthanoids are doped together in the same matrix.[37,38] Separation of the Tm^{3+} and Nd^{3+} ions, through the design of core−shell structures, prevents cross-relaxation.[35,37] Further enhancement of the upconversion efficiency can be achieved by the addition of an undoped $NaYF_4$ outer shell to the UCNPs, which prevents surface-based excited-state quenching processes, in particular in aqueous solution.[39] To effectively shield the inner core of the UCNP from the surface, the formation of an epitaxial shell is crucial, which can be done as proposed by van Veggel et al., by using small sacrificial nanoparticles (SNPs) as precursors.[40,41]

Recently, the groups of Salassa and Wu demonstrated that ligand-photodissociation reactions in ruthenium polypyridyl complexes can be triggered by a combination of UCNPs and 980 nm light, thus providing an important proof of concept for UCNP-mediated PACT.[25,42] Furthermore, several groups have reported encouraging preliminary results on the biological effects of ruthenium-based phototherapeutic agents conjugated to the surface of (upconverting) nanomaterials.[13,43,44] Nevertheless, despite the known disadvantages of 980 nm irradiation, very few reports exist that employ the more biocompatible 800 nm irradiation wavelength for the activation of ruthenium complexes.[45,46] In addition, many different strategies may be chosen for coupling the complex to the UCNP surface because there is relatively little knowledge on how to optimize both the dispersibility in aqueous solution and the energy transfer from the UCNP to the complex.

First, to ensure efficient activation of the ruthenium complex by the UCNP, the spectral overlap between the ruthenium complex and the UCNP emission should be maximized. Here, thulium-doped nanoparticles were selected for the superior spectral overlap of their emission with the absorption maximum of most ruthenium complexes (between 400 and 500 nm). Furthermore, minimization of the distance between the upconverting donor and the ruthenium acceptor can be achieved through direct binding of the ruthenium complex to the UCNP surface.[47]

Successful strategies for increasing the dispersibility of UCNPs in aqueous media include the so-called "ligand exchange" strategies, in which the oleate ligands are replaced by more strongly bound, hydrophilic capping ligands.[48,49] Because the stability of the binding of capping ligands to the UCNP surface is typically governed by the basicity of the binding moiety as well as the denticity of the surface-binding capping ligands, strong binding is accomplished using hard, poorly basic, anionic coordinating moieties, e.g., phosphonates, and the binding strength can be further enhanced by employing multidentate capping ligands.[50,51]

We envisioned that, through the careful design of a small organic ligand, we could address several of the challenges described above. Ligand $\mathbf{3_H}$ combines two soft thioether groups for selective, photolabile coordination to ruthenium(II),[52,53] with hard anionic phosphonate moieties to bind the UCNP surface. The use of a bidentate phosphonate increases the resistance to substitution of the phosphonates by ions from the buffer, whereas the relatively small size of $\mathbf{3_H}$, together with a set of thin shell layers on the UCNP, ensures close proximity (<2 nm) of the ruthenium center to the thulium ions in the UCNP core.

In this work, we report the synthesis of ruthenium-modified, H_2O-dispersible $NaYF_4$:Yb^{3+},Tm^{3+}@$NaYF_4$:Nd^{3+}@$NaYF_4$ core−shell−shell UCNPs (CSS-UCNP@[**1**]) by exchanging the surface ligands of the nanoparticle for the novel photoactivatable ruthenium(II) polypyridyl complex $[Ru(bpy)_2(\mathbf{3_H})](PF_6)_2$ ($[\mathbf{1}](PF_6)_2$), where bpy = 2,2-bipyridine. We describe the nanoparticle synthesis, the synthesis and aqueous photochemistry of the ruthenium complex, and the conjugation of the complex to the nanoparticle surface, providing the first systematic study of the effect of pH on the efficiency of the UCNP surface coating with a ruthenium phosphonate complex. Moreover, photoactivation of the CSS-UCNP@[**1**] nanoconjugate in H_2O (Scheme 1) under 800 nm irradiation is described.

https://dx.doi.org/10.1021/acs.inorgchem.0c00043
Inorg. Chem. 2020, 59, 14807−14818

Scheme 2. Synthesis Schemes for the Preparation of (A) α-$NaYF_4$:Nd^{3+} or α-$NaYF_4$ SNPs and (B) β-$NaYF_4$:Yb^{3+},Tm^{3+}@$NaYF_4$:Nd^{3+}@$NaYF_4$ CSS-UCNPs[a]

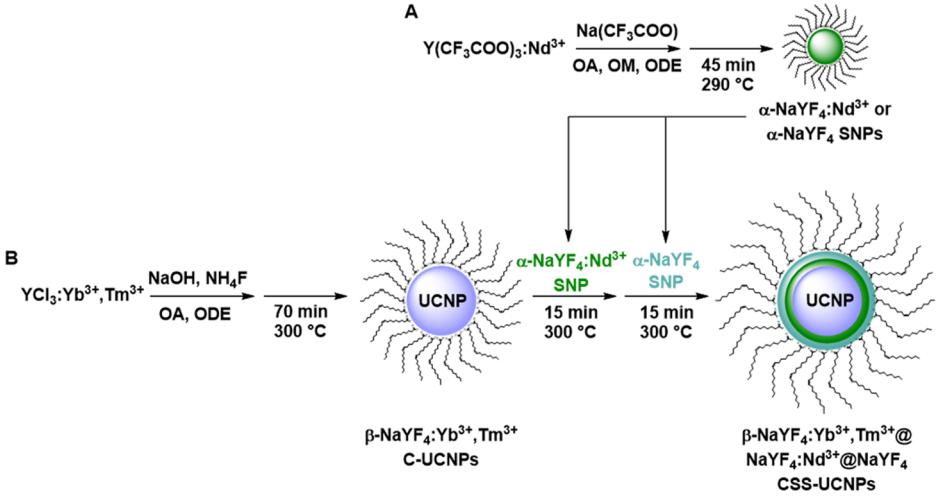

[a]OA = oleic acid, OM = oleylamine, and ODE = 1-octadecene.

RESULTS AND DISCUSSION

Synthesis and Characterization of UPNPs. Monodisperse $NaYF_4$:Yb^{3+},Tm^{3+}@$NaYF_4$:Nd^{3+}@$NaYF_4$ CSS-UCNPs were synthesized according to a single-step self-focusing strategy (Scheme 2B), employing SNPs as the shell precursor material.[40] These SNPs were produced through a thermal decomposition method, using trifluoroacetate precursors (Scheme 2A). The SNPs were found to be ca. 6 nm in diameter and of pure cubic (α) phase, as shown by transmission electron microscopy (TEM; Figure S1) and powder X-ray diffraction (XRD; Figure S2). The percentage of organic capping ligands was determined via thermogravimetric analysis (TGA; Figure S3). SNPs were prepared both with and without neodymium doping, to serve as precursors for the first and second shells, respectively.

The nanoparticle core, consisting of the hexagonal phase β-$NaYF_4$, doped with Yb^{3+} (20%) and Tm^{3+} (0.5%) ions, was prepared from a chloride precursor salt, optimizing a procedure described previously.[54] At the end of the ripening phase, the nanoparticle dispersion was kept stirring at 300 °C, and a dispersion of α-$NaYF_4$ SNPs, doped with Nd^{3+} (20%) ions, in 1-octadecene was injected. Upon injection, the smaller cubic SNPs dissolved and ripened on the surface of the core nanoparticles as an epitaxial, hexagonal-phase shell. This process was repeated once more, using undoped α-$NaYF_4$ SNPs, resulting in a second, undoped shell layer. After workup, the oleate-capped CSS-UCNPs were characterized by TEM, XRD, TGA, and inductively coupled plasma optical emission spectroscopy (ICP-OES) (Figures 1 and S2 and S3 and Table S1). Samples taken of the core and core–shell intermediates were also examined by TEM and ICP-OES to determine the shell thickness and the dopant concentrations of the various layers. The CSS-UCNPs were determined to be of almost spherical morphology and 41.3 ± 1.5 nm in diameter, with shell thicknesses of 1.8 and 1.4 nm for the first and second shells, respectively. The total shell thickness of 3.5 nm is close to the optimal shell thickness reported for efficient energy transfer to surface-bound acceptors.[47]

To further confirm the successful formation of the shell layers, we examined the emission of the oleate-capped core (C-), core–shell (CS-), and CSS-UCNPs in toluene under

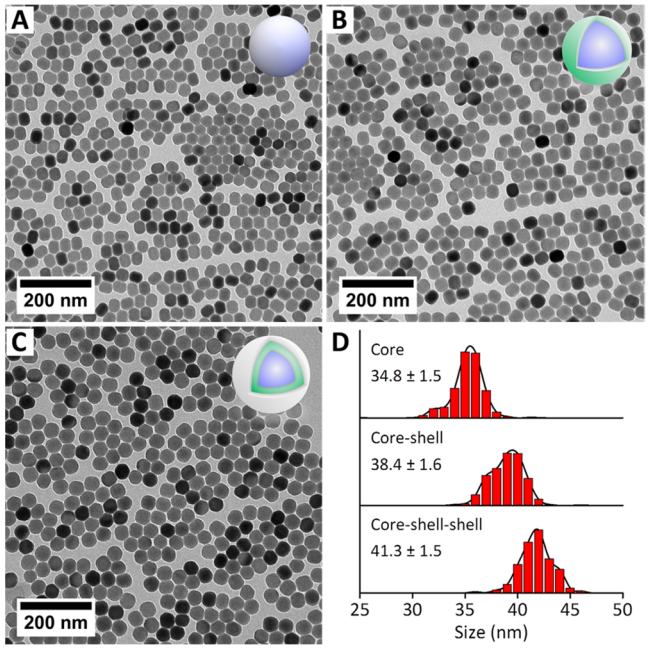

Figure 1. (A–C) TEM images of (A) $NaYF_4$:Yb^{3+},Tm^{3+} C-UCNPs, (B) $NaYF_4$:Yb^{3+},Tm^{3+}@$NaYF_4$:Nd^{3+} CS-UCNPs, and (C) $NaYF_4$:Yb^{3+},Tm^{3+}@$NaYF_4$:Nd^{3+}@$NaYF_4$ CSS-UCNPs. (D) Histograms of the particle-size distributions of the nanoparticle samples, as determined by TEM.

both 796 and 969 nm excitation (Figure 2C,D). Because of the presence of the Yb^{3+} ions in the core, excitation of all three types of UCNPs can be done using 969 nm, resulting in the typical blue thulium-based emission (Figure 2B). The upconverted emission spectra display multiple emission bands, all corresponding to Tm^{3+} 4f–4f transitions (Figure 2A), at 451 nm ($^1D_2 \rightarrow {}^3F_4$), 475 nm ($^1G_4 \rightarrow {}^3H_6$), 509 nm ($^1D_2 \rightarrow {}^3H_5$), 647 nm ($^1G_4 \rightarrow {}^3F_4$), 698 and 740 nm ($^3F_{2,3} \rightarrow {}^3H_6$), and 802 nm ($^1G_4 \rightarrow {}^3H_5$ and $^3H_4 \rightarrow {}^3H_6$). The higher-energy emission bands in the UV, most notably those at 345 and 365 nm, could not be detected because of the optical filters used in blocking the scattered excitation light. Under 969 nm

https://dx.doi.org/10.1021/acs.inorgchem.0c00043
Inorg. Chem. 2020, 59, 14807–14818

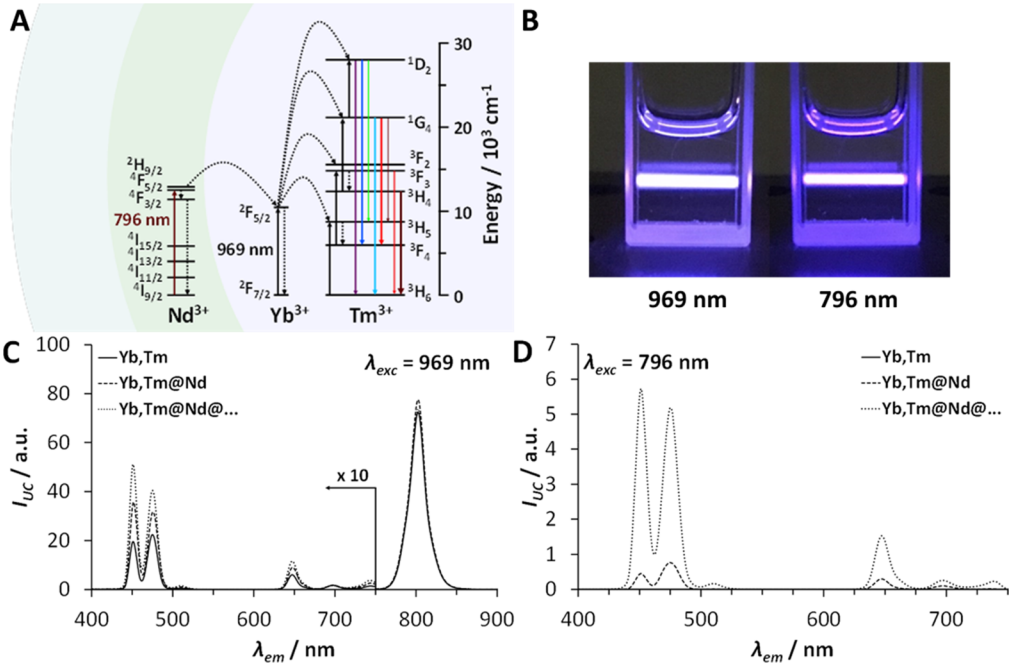

Figure 2. (A) Simplified energy-level diagram depicting the energy-transfer upconversion mechanism in the CSS-UCNPs for excitation using 796 and 969 nm light and assignment of the thulium emission lines. (B) Photographs of the upconverted emission under 969 nm (left) and 796 nm (right) excitation in toluene. Upconverted emission spectra under 969 nm (C) and 796 nm (D) excitation in toluene (P_{exc} = 50 W·cm^{-2}, T = 293 K, and [UCNP] = 1 mg·mL^{-1}). The emission between 400 and 750 nm under 969 nm excitation is enhanced by a factor of 10 for clarity.

excitation (Figure 2C), the addition of the first, neodymium-doped shell leads to a 60% increase in the emission intensity of the blue emission bands at 450 and 475 nm. The addition of the second, undoped shell results in a similar enhancement of the blue emission, making for a 2.2-fold total enhancement of the blue emission, on going from C- to CSS-UCNPs. The enhancement is smaller than that observed for similar CS systems that have only undoped shells[40,55] because the shell added here is relatively thin and because the neodymium introduced in the first shell can act as a quencher for the thulium emission through cross-relaxation, thereby partially canceling out the increase in emission caused by the prevention of surface quenching.[37]

No upconverted emission signal was observed from the C-UCNPs under 796 nm irradiation (Figure 2D) because these did not contain the neodymium sensitizer necessary to absorb this light. As expected, the CS-UCNPs did show blue emission under 796 nm excitation, albeit ca. 5-fold less intense than the blue emission under 969 nm at the same power density, caused by the close proximity of the Nd^{3+} ions to the nanoparticle surface and, hence, the efficient surface quenching. However, the addition of the second, undoped shell leads to an 8-fold enhancement in blue emission over the CS-UCNPs. Overall, the blue emission of the CSS-UCNPs was found to be 20% more intense under 796 nm excitation than under 969 nm excitation (Figure 2C,D) at the same excitation power density. This difference in the emission intensity is most likely primarily caused by a more efficient absorption of the excitation light by Nd^{3+} ions (under 796 nm irradiation), compared to Yb^{3+} (under 969 nm irradiation).[35]

Synthesis of the Ruthenium Complex [1](PF$_6$)$_2$. To functionalize the CSS-UCNPs with a photoactivatable ruthenium polypyridyl complex, a ligand was designed that offered hard donor atoms for interacting with the hard lanthanoid ions of the nanoparticles and a soft, bidentate thioether ligand to bind to and protect the soft ruthenium center. Ligand $\mathbf{3}_{Et}$, containing two protected phosphonate moieties, was obtained in three steps from commercially available 1,3-bis(methylthio)-2-propanol, as shown in Scheme 3. Coordination of this ligand to ruthenium was performed using the protected ligand, in order to prevent any undesired reactions between the deprotected phosphonates and the ruthenium center. The successful synthesis of the protected complex [Ru(bpy)$_2$($\mathbf{3}_{Et}$)](PF$_6$)$_2$ ([**6**](PF$_6$)$_2$) was achieved by refluxing the ruthenium precursor complex *cis*-[Ru(bpy)$_2$Cl$_2$] with a slight excess of ligand $\mathbf{3}_{Et}$ in H_2O, followed by anion exchange using KPF_6. Deprotection of the phosphonate groups was done using a large excess of trimethylsilyl bromide (TMSBr) in dichloromethane (DCM), yielding [**1**](PF$_6$)$_2$ in a total of five steps in 17% overall yield. In the aliphatic region of the ^{1}H NMR spectrum in CD_3OD, complete coordination of the two sulfur atoms to the ruthenium center was confirmed by the disappearance of the singlet peak at 2.14 ppm for the uncoordinated thiomethyl groups of $\mathbf{3}_{Et}$. Elemental analysis confirmed that [**1**](PF$_6$)$_2$ and [**6**](PF$_6$)$_2$ were isolated as their bis(hexafluoridophosphate) salt. Despite the presence of this apolar anion, compounds [**1**](PF$_6$)$_2$ and [**6**](PF$_6$)$_2$ were both found to be soluble in H_2O. Both complexes were characterized using NMR spectroscopy, high-resolution mass spectrometry, elemental analysis, thin-layer chromatography, Fourier transform infrared (FT-IR) spectroscopy, and UV−vis absorption spectroscopy (vide infra).

Upon coordination of ligand $\mathbf{3}_{Et}$ to the ruthenium center through its two sulfur atoms, a six-membered ring is formed. The methyl groups adjacent to these sulfur atoms appear in the ^{1}H NMR spectrum of [**1**](PF$_6$)$_2$ as two separate singlet signals (at 1.43 and 1.31 ppm in CD_3OD), indicating the non-equivalence of these groups in [**1**](PF$_6$)$_2$. This inequivalence results from the conformational constraints imposed by formation of the metallacycle, which introduce several sources

https://dx.doi.org/10.1021/acs.inorgchem.0c00043
Inorg. Chem. 2020, 59, 14807−14818

Scheme 3. Synthesis of the Ruthenium Complex $[1](PF_6)_2$[a]

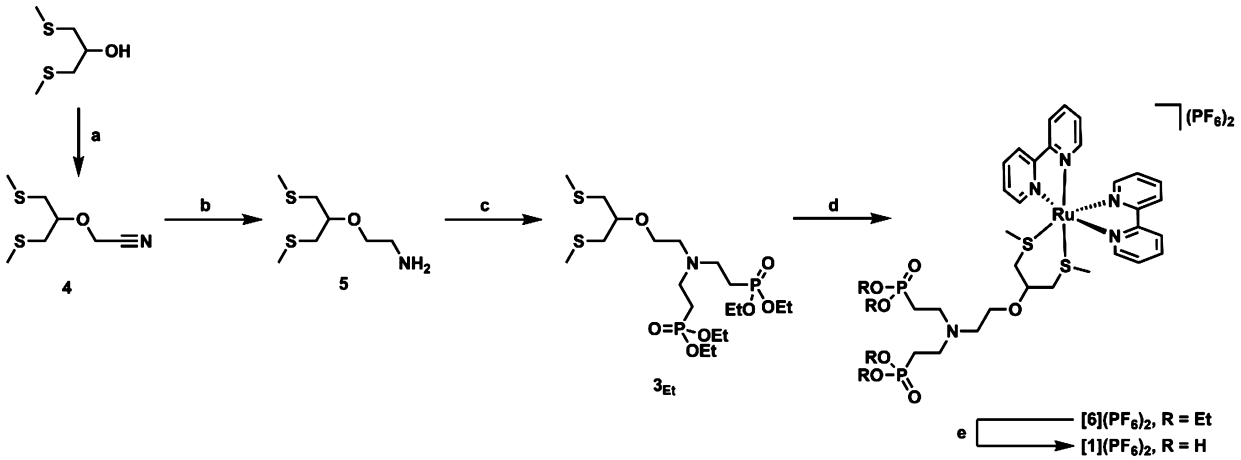

[a]Conditions: (a) NaH, KI, chloroacetonitrile in CH_3CN, 0 °C to RT, 24 h, 30%; (b) $LiAlH_4$ (1 M in tetrahydrofuran) in diethyl ether, 0 °C to RT, 5 h, quantitative; (c) diethyl vinylphosphonate in H_2O, RT, 5 days, 75%; (d) (i) *cis*-$[Ru(bpy)_2Cl_2]$ in H_2O, reflux, 1.5 h; (ii) KPF_6, 80%; (e) TMSBr in DCM, RT, 16 h, 93%. Compounds $[1](PF_6)_2$ and $[6](PF_6)_2$ were obtained as racemic Λ/Δ mixtures.

Table 1. Lowest-Energy Absorption Maxima (λ_{max}), Molar Absorption Coefficients at λ_{max} (ε_{max}) and 445 nm (ε_{445}), Photosubstitution Quantum Yields (Φ_{445}), and Photosubstitution Reactivities ($\xi_{445} = \Phi_{445}\varepsilon_{445}$) at 298 K in H_2O and Singlet Oxygen Quantum Yields (Φ_Δ) and Phosphorescence Quantum Yields (Φ_P) at 293 K in MeOD for Complexes $[1](PF_6)_2$ and *cis*-$[Ru(bpy)_2(\kappa^1\text{-}3_H)(H_2O)](PF_6)_2$ ($[7](PF_6)_2$)

complex	λ_{max}/nm (ε_{max}/$M^{-1}\cdot cm^{-1}$)	ε_{445}/$M^{-1}\cdot cm^{-1}$	Φ_{445}	ξ_{445}	Φ_Δ	$\Phi_P(\lambda_{em}$/nm)
$[1](PF_6)_2$	415 (5.10×10^3)	3.52×10^3	0.12	422	0.011	1.4×10^{-4} (616)
$[7](PF_6)_2$	456 (6.46×10^3)	6.11×10^3	0.0051	31		

Scheme 4. Two-Step Photoreaction Observed upon Blue-Light Irradiation of a Solution of $[1]^{2+}$ in H_2O

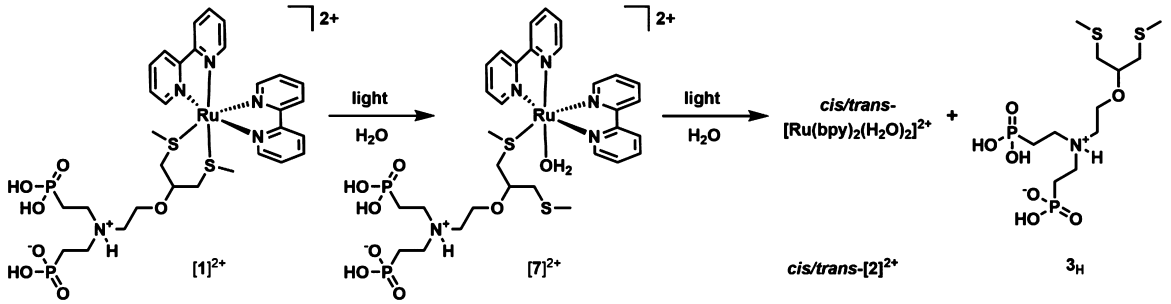

of isomerism on top of the preexisting chirality of the octahedron (Λ or Δ), namely, the configuration of the two ruthenium-coordinated sulfur atoms (*R* or *S*) and the carbon atom (*R* or *S*) adjacent to the ether substituent. As a result of the symmetrical design of the ligand, chair inversion does not lead to another different set of isomers, bringing the total number of possible isomers to eight Λ diastereoisomers plus their corresponding Δ enantiomers. The potential isomers of this class of ruthenium thioether complexes were described by us recently.[56] According to 1D and 2D ^1H NMR, which showed only a single set of 16 aromatic proton signals originating from the bipyridine ligands, both complexes $[1](PF_6)_2$ and $[6](PF_6)_2$ were obtained as single diastereoisomers.

Photochemistry and Thermal Stability of $[1](PF_6)_2$. In aqueous solution, $[1](PF_6)_2$ showed a ^{1}MLCT absorption band around 415 nm, with a molar absorptivity of ~5100 $M^{-1}\cdot cm^{-1}$ (Table 1), typical for ruthenium(II) polypyridyl complexes containing two thioether donor ligands.[53] The complex was found to be only weakly emissive at room temperature under air (phosphorescence quantum yield $\Phi_P = 1.4 \times 10^{-4}$), with similarly low singlet-oxygen-generation quantum yields ($\Phi_\Delta = 0.011$; Figure S4) under air.

The photoreactivity of $[1](PF_6)_2$ in H_2O (pH 3.7) was monitored using UV−vis absorption spectroscopy and mass spectrometry. Under these conditions, the complex is assumed to exist in a zwitterionic form as a result of the basicity of the tertiary amine located in the aliphatic ligand (Scheme 4). In the dark at 25 °C, no changes to the absorption spectrum of an aqueous solution of $[1](PF_6)_2$ were observed overnight (Figure S5), showing that the complex is thermally stable. In contrast, under irradiation with blue light ($\lambda = 445 \pm 11$ nm), the absorbance of the solution showed a two-step bathochromic shift (Figures 3 and S6). First, the absorption maximum shifted from 415 to 456 nm, with clear isosbestic points at 319, 361, and 426 nm (Figure 3A). After about 7 min, the absorption maximum started to display a further shift from 456 to 492 nm, accompanied by the appearance of new isosbestic points at 332, 391, and 466 nm (Figure 3B). This second change in the absorption maximum happened

https://dx.doi.org/10.1021/acs.inorgchem.0c00043
Inorg. Chem. 2020, 59, 14807−14818

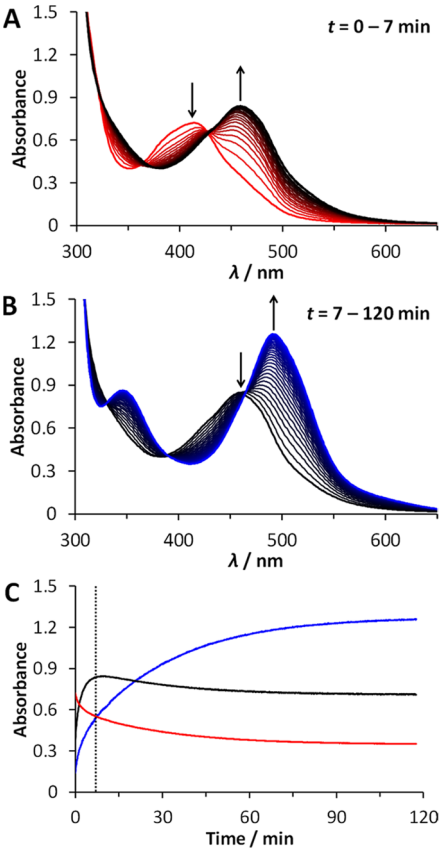

Figure 3. Evolution in time of the UV–vis absorption spectra of a solution of $[\mathbf{1}](PF_6)_2$ in H_2O (0.129 mM) upon irradiation at 298 K with a 445 nm light-emitting diode ($q_p = 3.71 \times 10^{-8}$ mol of photons·s^{-1}) under N_2 for t = 0–7 min (A, Δt = 0.2 min) and t = 7–120 min (B, Δt = 3.2 min) and the time evolution of the absorbance (C) at 415 nm (red), 456 nm (black) and 492 nm (blue) during irradiation. The vertical dashed line (t = 7 min) indicates completion of the first reaction.

considerably more slowly than the first change, taking approximately 2 h to complete. Mass spectrometry of the reaction mixture after 120 min of irradiation (Figure S7) showed a peak at m/z 247.7, corresponding to $[Ru(bpy)_2(CH_3CN)_2]^{2+}$ (calcd m/z 248.0), formed inside the mass spectrometer from the original photoproduct $[Ru(bpy)_2(OH_2)_2]^{2+}$ ($[\mathbf{2}]^{2+}$), and indicating that, upon blue-light irradiation of $[\mathbf{1}]^{2+}$ in H_2O, the bis(thioether) chelate $\mathbf{3_H}$ is selectively substituted by two H_2O molecules. The photoreleased ligand $\mathbf{3_H}$ could not be observed by mass spectrometry because of its negative charge under the conditions used.

In order to identify the intermediate species in the photoreaction, mass spectrometry was also performed after the first 10 min of irradiation (Figure S8). Besides peaks at m/z 412.4 and 247.9, corresponding to the starting complex $[\mathbf{1}]^{2+}$ (calcd m/z 412.6) and the photoproduct $[Ru(bpy)_2(CH_3CN)_2]^{2+}$ (calcd m/z 248.0), two more peaks were found, at m/z 421.5 and 433.1, matching with $[Ru(bpy)_2(\mathbf{3_H})(OH_2)]^{2+}$ (calcd m/z 421.6) and $[Ru(bpy)_2(\mathbf{3_H})(CH_3CN)]^{2+}$ (calcd m/z 433.1). Considering the stability of the intermediate species, it is most likely six-coordinate, with ligand $\mathbf{3_H}$ bound through one of its two thioether donors and the other one replaced by a H_2O molecule, i.e., *cis*-$[Ru(bpy)_2(\kappa^1\text{-}\mathbf{3_H})(OH_2)]^{2+}$ ($[\mathbf{7}]^{2+}$). All in all, under blue-light irradiation, $[\mathbf{1}](PF_6)_2$ undergoes a two-step consecutive photochemical substitution of the bis(thioether) ligand, passing through the rather stable monoaqua intermediate $[\mathbf{7}]^{2+}$ (Scheme 4). This two-step photoreactivity is strictly similar to that reported previously for the complex $[Ru(bpy)_2(bmtp)](PF_6)_2$, where bmtp = 1,3-bis(methylthio)-propanol.[56] The quantum efficiencies of the two photochemical steps were derived using global fitting of the time evolution of the UV–vis absorption spectra, using the *Glotaran* software package.[57] The photosubstitution quantum yields were found to be 0.12 for the first step and 0.0051 for the second one (Table 1 and Figure S9).

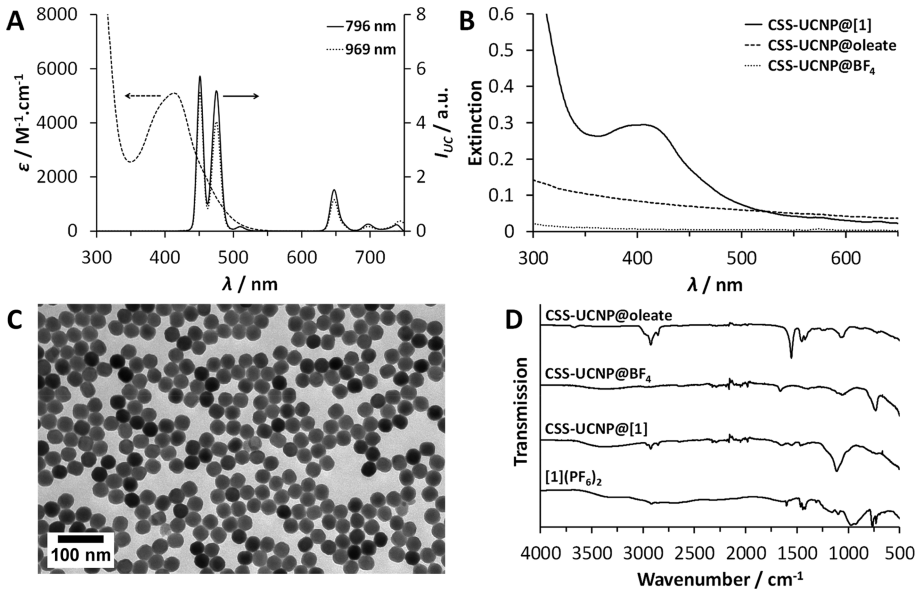

Figure 4. (A) Overlap between the UV–vis absorption spectrum of $[\mathbf{1}](PF_6)_2$ in H_2O (dashed line) and the emission of CSS-UCNPs in toluene under 796 nm (solid line) and 969 nm (dotted line) excitation. (B) UV–vis absorption spectrum of CSS-UCNP@oleate in cyclohexane (dashed line), CSS-UCNP@BF_4 in DMF (dotted line), and CSS-UCNP@[**1**] in H_2O (solid line). (C) TEM micrograph of CSS-UCNP@[**1**] in H_2O. (D) FT-IR spectra of CSS-UCNP@oleate, CSS-UCNP@BF_4, CSS-UCNP@[**1**], and $[\mathbf{1}](PF_6)_2$.

https://dx.doi.org/10.1021/acs.inorgchem.0c00043
Inorg. Chem. 2020, 59, 14807–14818

Scheme 5. Synthesis of CSS-UCNP@[1] by Surface Ligand Exchange

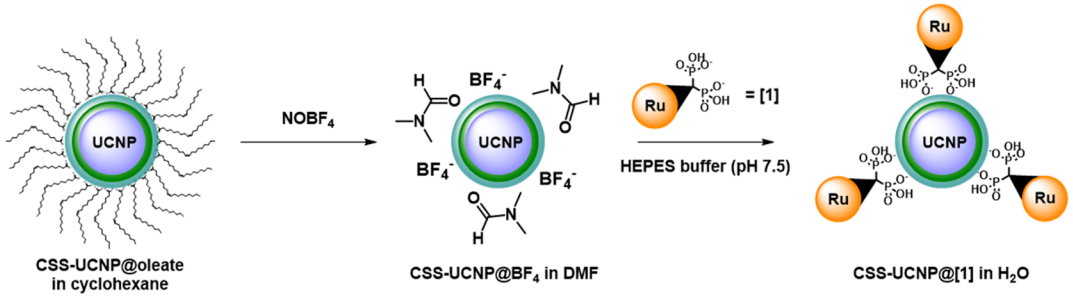

Synthesis and Characterization of CSS-UCNP@[1]. Figure 4A shows that the spectral overlap between the absorption spectrum of the complex $[\mathbf{1}](PF_6)_2$, and the emission spectrum of the thulium-doped CSS-UCNPs is good, under both 796 and 969 nm excitation, an important condition for the activation of $[\mathbf{1}](PF_6)_2$ using the UCNP emission. The oleate-capped CSS-UCNPs are initially only dispersible in hydrophobic media, while $[\mathbf{1}](PF_6)_2$ is insoluble in these solvents because of the strongly hydrophilic phosphonate ligands. Therefore, an intermediate step was necessary to bring both components in a common medium and realize the surface coating of CSS-UCNPs with the ruthenium complex (Scheme 5). Inspiration for the use of a weakly bound tetrafluoridoborate anion as an intermediate surface coating and *N*,*N*-dimethylformamide (DMF) as a medium of intermediate polarity was drawn from Dong et al.[58] Replacement of the BF_4^- anions could be accomplished by mixing a DMF dispersion of the BF_4-coated CSS-UCNPs (CSS-UCNP@BF_4) with a neutral aqueous solution of [**1**] and stirring it overnight, followed by centrifugal washing to remove the excess ruthenium complex, to obtain CSS-UCNP@[**1**] in an aqueous dispersion. Photographs of the purification process are provided in Figure S12. CSS-UCNP@[**1**] was stored in a dispersed form in Milli-Q H_2O, and the dispersion was found to be stable for several days. Any sediment observed could be easily redispersed using mild sonication for several minutes.

The ligand-exchange procedure was monitored using multiple spectroscopic techniques at various stages of the procedure. UV−vis absorption spectra (Figure 4B) were measured before exchange (CSS-UCNP@oleate), after removal of the oleate ligands (CSS-UCNP@BF_4), and for the final nanoconjugate (CSS-UCNP@[**1**]). In the spectrum of the final nanoconjugate, a peak appeared around 400 nm (solid line in Figure 4B), matching well with the absorption spectrum of $[\mathbf{1}](PF_6)_2$ shown in Figure 4A. The various stages of the ligand exchange were also monitored using FT-IR spectroscopy, as depicted in Figure 4D. Removal of the oleate ligands can be clearly observed in the first step by the disappearance of the peaks at 2924, 2856, 1556, and 1452 cm^{-1}, which originate from the asymmetric and symmetric C−H and O═C−O stretching modes in surface-bound oleates, respectively.[17,59] The small peaks appearing at 1660 and 1057 cm^{-1} are attributed to the C═O and B−F stretch modes in DMF and BF_4^-, respectively.[58] Upon introduction of the ruthenium phosphonate complex, these peaks are replaced by a strong broad peak of the phosphonate stretching mode around 1112 cm^{-1}. The ruthenium-coated nanoparticles were well dispersible in H_2O, as shown by TEM (Figure 4C), but they formed small aggregates, as indicated by dynamic light scattering (DLS; Figure S10), characterized by an average hydrodynamic size of 115 nm. The ζ potential of CSS-UCNP@[**1**] was found to be positive (32 ± 6 mV), confirming the presence of positively charged ruthenium complexes on the surface of the nanoparticles (Figure S11).

It is worth pointing out that the protonation state of the phosphonate groups in complex [**1**] plays an important role in the binding of [**1**] to the UCNP surface. Because the interaction between the UCNPs and these ligands is mostly electrostatic in nature,[49] deprotonation of the phosphonate groups leads to a stronger coordination to the surface. With changes in the pH in aqueous media, the overall charge of complex [**1**] can vary between 3+ and 2− as a result of the protonation state of its two phosphonate groups and its basic tertiary amine. However, because none of these protonation steps influences the energy level of the ^{1}MLCT absorption band, which is believed to be delocalized over the metal center and the bpy ligands,[53] the UV−vis absorption spectrum is not affected by the pH, precluding a photophysical determination of the pK_a values of [**1**].

Rather than performing cumbersome titration studies to determine the pK_a values of $[\mathbf{1}]^{2+}$, we determined the optimal pH for the UCNP coating by performing the ligand-exchange process in three different Good's buffers,[60] over a pH range from 6.1 to 8.4, specifically 2-(*N*-morpholino)ethanesulfonic acid (MES; pK_a = 6.1), 4-(2-hydroxyethyl)-1-piperazineethanesulfonic acid (HEPES; pK_a = 7.5), and *N*-tris(hydroxymethyl)methyl-3-aminopropanesulfonic acid (TAPS; pK_a = 8.4). All buffers were used at pH values around their respective pK_a to maximize their buffering capacity. The use of phosphate buffers was avoided because these are strongly competing with UCNP surface ligands, and they are known to be able to cause particle dissolution upon prolonged exposure.[50,61] ICP-OES was used to determine the yttrium and ruthenium concentrations in the nanoconjugates, which could be used to estimate the number of molecules of [**1**] per UCNP (Table 2). The yttrium concentration was found to be similar across all buffers used, proving that the amount of CSS-UCNPs recovered after the ligand-exchange procedure (the UCNP yield) was constant at ∼60%. However, the ruthenium concentration in the samples was found to strongly increase with increasing pH from 6.1 to 7.5, most likely as a result of deprotonation of the phosphonate ligands of complex [**1**]. No further improvement of the ruthenium binding was observed when the pH was further increased to 8.4 using TAPS buffer. To exclude the possibility that the nature of the buffering agent plays a role in the coating efficiency, the experiment was repeated in Milli-Q H_2O, basified to a similar pH using NaOH (Table 2, entries 4−6). Similar trends were observed here, confirming that the coating efficiency depends solely on the

https://dx.doi.org/10.1021/acs.inorgchem.0c00043
Inorg. Chem. 2020, 59, 14807−14818

Table 2. pH Effects on the Synthesis of CSS-UCNP@[1][a]

entry	solvent	pH	CSS-UCNP yield/%	Ru/CSS-UCNP ($\times 10^3$)	ligand density/nm^{-2}	Ru coating yield/%
1	MES buffer	6.1	60	1.4 ± 0.2	0.27 ± 0.04	4
2	HEPES buffer	7.5	63	2.37 ± 0.09	0.44 ± 0.04	7
3	TAPS buffer	8.4	56	2.37 ± 0.08	0.44 ± 0.04	6
4	H_2O	6.3	68	0.82 ± 0.06	0.15 ± 0.02	2
5	H_2O	7.9	59	2.27 ± 0.09	0.42 ± 0.04	6
6	H_2O	9.0	55	2.26 ± 0.07	0.42 ± 0.03	6

[a]Errors indicate the uncertainty in the ICP-OES concentration determination, with sample digestion performed in triplicate and ICP-OES measurements performed in duplicate.

pH of the solution and not on the nature of the counteranion in the buffer.

Finally, HEPES buffer at pH 7.5 was selected as the optimal medium for the ligand-exchange procedure, yielding ~2.4 × 10^3 ruthenium complexes bound per 41 nm nanoparticle. This corresponds to a surface area of 2.3 ± 0.2 nm^2 per ruthenium complex or a ligand density of 0.44 ± 0.04 nm^{-2}. Earlier work on the functionalization of UCNPs with monophosphonate ruthenium complexes reports similar amounts of ruthenium per UCNP (~3000 per UCNP for 37 nm UCNPs).[62] On the other hand, the ligand density found is much smaller than the value reported by Tong et al. for organic PEGylated tetraphosphonate (1.8 nm^{-2}) or monophosphate (1.5 nm^{-2}) surface ligands.[63] Because of the small footprint of this tetraphosphonate ligand, the authors stated that it is likely to be bound with less than two of its four phosphonates simultaneously. The low ligand density observed for CSS-UCNP@[**1**] could be explained by the simultaneous coordination of both phosphonate moieties, leading to a larger footprint of the surface ligand, or, most likely, by the large bulk and close proximity of the ruthenium polypyridyl group, blocking access to the nanoparticle surface. The ruthenium surface coverage is not limited by the amount of ruthenium added during the ligand exchange because less than 10% of the total ruthenium added during UCNP functionalization eventually ended up on the nanoparticle surface (see the ruthenium coating yields in Table 2).

Photoactivation of CSS-UCNP@[1]. CSS-UCNP@[**1**] can decompose by dissociation of the bis(phosphonate) ligand from the nanoparticle surface or by dissociation of the sulfur ligand from the ruthenium center. The dark stability of CSS-UCNP@[**1**] in H_2O was monitored using UV−vis absorption spectroscopy and DLS, performed directly after preparation of the nanoconjugate or after 9 h in the dark at room temperature. Clearly, no significant changes to the absorption spectra were observed (Figure S13B), indicating that no unbinding of the sulfur ligand from the ruthenium complex had taken place in the dark. Furthermore, no changes were observed in the hydrodynamic particle size or the ζ potential (Figures S10 and S11), suggesting that the phosphonate remained bound to the nanoparticle surface in the dark. Overall, the CSS-UCNP@[**1**] nanoconjugates appeared to be stable in the dark over several days at room temperature.

Upon irradiation of CSS-UCNP@[**1**] with a 796 nm continuous-wave (CW) laser for 6 h, a clear bathochromic shift was observed in the UV−vis absorption spectra (Figure 5A). During the first 150 min, the absorption band around 405 nm disappeared, while a new band at 457 nm appeared, with isosbestic points around 323 and 431 nm. This change was similar to the first step of the photochemical reaction of $[\mathbf{1}]^{2+}$ under blue-light irradiation in aqueous solution, i.e., formation

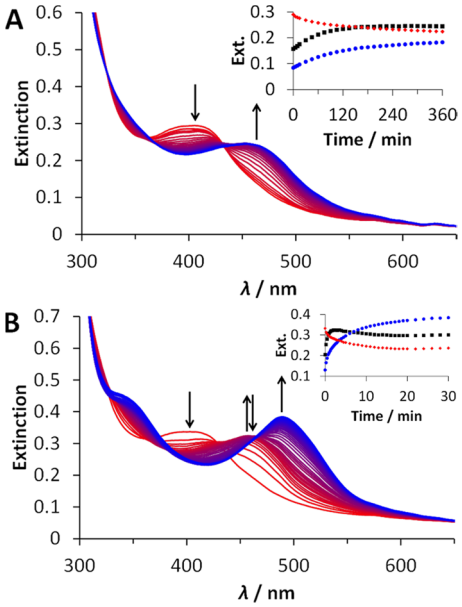

Figure 5. (A and B) Evolution of the UV−vis absorption spectra of a dispersion of CSS-UCNP@[**1**] in aerated H_2O ([CSS-UCNP] ≈ 14 nM, 1.6 mg·mL^{-1}, and T = 25 °C) upon irradiation with (A) a 796 nm CW laser beam (2.0 W, 50 W·cm^{-2}) for 360 min and (B) a 450 nm CW laser beam (10 mW, 0.080 W·cm^{-2}) for 30 min. Inset: Time evolution of the extinction at 415 nm (red diamonds), 456 nm (black squares), and 492 nm (blue circles) during irradiation.

of $[\mathbf{7}]^{2+}$ (Figure 3A). After 2.5 h, the isosbestic point at 431 nm disappeared, and the absorption maximum at 457 nm began to shift toward slightly higher wavelengths. We attribute these slower changes to the second step of the ruthenium-based photosubstitution reaction, i.e., conversion of CSS-UCNP@[**7**] into $[\mathbf{2}]^{2+}$, and the release of this ruthenium complex from the UCNP surface. After 6 h, the sample was centrifuged, and the supernatant and pellet were separately dissolved in H_2O. UV−vis absorption spectra were recorded for both the pellet fraction and the supernatant (Figure S14). A clear agreement was observed between the lowest-energy absorption peak in the supernatant fraction and the known ^{1}MLCT absorption peak of $[\mathbf{2}]^{2+}$ around 490 nm. Thus, the photochemically generated bis(aqua) complex was released from the UCNP surface. A shoulder between 400 and 500 nm was seen in the absorption spectrum of the pellet fraction containing the CSS-UCNPs, matching the absorption features of the ruthenium complexes $[\mathbf{1}]^{2+}$ and, to a greater extent, $[\mathbf{7}]^{2+}$. This indicates that the photochemical conversion of the ruthenium complex $[\mathbf{1}]^{2+}$ via $[\mathbf{7}]^{2+}$ into $[\mathbf{2}]^{2+}$ was not completed within 6 h of irradiation and that the remaining amounts of $[\mathbf{1}]^{2+}$ and $[\mathbf{7}]^{2+}$ were left bound to the UCNP

https://dx.doi.org/10.1021/acs.inorgchem.0c00043
Inorg. Chem. 2020, 59, 14807−14818

surface through their thioether ligand. From the UV−vis extinction spectrum of the supernatant after NIR irradiation, assuming that 40−80% of the observed extinction comes from absorption by ruthenium complex $[2]^{2+}$ and the rest is caused by nanoparticle-induced scattering, we can estimate that ∼5−10% of the ruthenium coating has been released from the surface of the nanoparticles. The incomplete photoreaction in this experiment is explained, of course, by the relatively low blue Tm^{3+} emission intensity generated by the four-photon upconversion process but also and primarily by the large difference in the photosubstitution reactivities ($\xi_{445} = \Phi_{445}\varepsilon_{445}$) between the first ($\xi_{445}$ = 422; Table 1) and second (ξ_{445} = 31) photosubstitution steps. According to these numbers, if one assumes that the upconverted blue-light intensity generated by the UCNP remains constant throughout the irradiation, the irradiation time required to complete the second photosubstitution reaction, and thus to fully detach the ruthenium complex from the nanoparticle surface, would be more than 10 times longer than that required for finishing the first photosubstitution step. Considering that in the conditions of this experiment this first step required several hours of irradiation to take place, it was not possible to push the second photoreaction to completion or to investigate the biological properties of CSS-UCNP@[**1**] nanoconjugates.

The efficiency of the photoactivation under 796 nm irradiation was compared to irradiation using 450 and 969 nm light (Figures 5B and S13A). Using the same excitation power density (50 W·cm^{-2}), the photosubstitution reaction rates under 796 and 969 nm irradiation were very similar, as was expected from the similar emission intensity found for the UCNPs in these cases (Figure 4A). As foreseen, direct excitation of the ruthenium complex, using light from a 450 nm laser, led to very efficient photoactivation of CSS-UCNP@[**1**]. Despite the low excitation power density (0.080 W·cm^{-2}), the photoreaction was completed within 30 min at 25 °C. After separation of the CSS-UCNP pellet from the supernatant, no ruthenium complex could be found on the CSS-UCNP fraction by UV−vis absorption spectroscopy (Figure S14). However, the supernatant fraction showed a clear absorption peak around 490 nm, indicative of the fully aquated species, i.e., $[2]^{2+}$, thus showing that the ruthenium photoproduct is released from the surface of the CSS-UCNPs upon photoactivation.

Evaluation of the colloidal stability and surface charge of the CSS-UCNPs after photoreaction confirmed the difference in the activation efficiency between the irradiation with 796 nm NIR light and direct activation using 450 nm light. After irradiation with the 450 nm laser, the positive surface charge had reduced significantly to 10 ± 4 mV, and the hydrodynamic particle size had increased to 450 nm, showing the formation of large aggregates (Figures S10 and S11). From this, we conclude that removal of the ruthenium complex from the UCNP surface leads to a decrease in the surface charge and the reduced electrostatic repulsion between the nanoparticles causes aggregation. In contrast, after 6 h of irradiation with the 796 nm laser, the surface charge had reduced negligibly, from 32 ± 6 to 30 ± 6 mV, and the hydrodynamic particle size had not changed significantly. This result implies that a significant fraction of the ruthenium complex is still present on the CSS-UCNP surface, most likely bound through only one of the two thioether groups, i.e., in the form of CSS-UCNP@[**7**], confirming the conclusions from the UV−vis absorption data. Overall, although photosubstitution of thioethers by H_2O in CSS-UCNP@[**1**] is clearly possible under 796 nm irradiation, an increase in the efficiency will be required to achieve full release of the ruthenium for therapeutically relevant conditions.

CONCLUSIONS

In this work, we have shown that a one-step synthesis method based on the injection of cubic-phase SNPs into a hot dispersion of C-UCNPs is a convenient method to produce $NaYF_4$:Yb^{3+},Tm^{3+}@$NaYF_4$:Nd^{3+}@$NaYF_4$ CSS-UPNPs with epitaxial shell layers and that these UCNPs are able to perform efficient photon upconversion under both 796 and 969 nm irradiation. The complex $[\mathbf{1}](PF_6)_2$, bearing the novel bis(phosphonate)bis(thioether) ligand $\mathbf{3_H}$, was shown to bind efficiently to the surface of CSS-UCNPs, stabilizing these UCNPs in aqueous dispersion. The binding of $[\mathbf{1}](PF_6)_2$ to the CSS-UCNP surface was found to be highly pH-dependent as a result of its acidic phosphonate residues. Optimally, coating should be performed at a neutral to slightly basic pH (7.5−9.0), resulting in full deprotonation of the phosphonate groups and thus an increase in the amount of ruthenium complex bound to the CSS-UCNP.

Importantly, the photoreactivity observed for $[\mathbf{1}](PF_6)_2$ in aqueous solution under blue-light irradiation can be triggered by NIR irradiation of CSS-UCNP@[**1**]. The incorporation of the neodymium-doped shell allowed for activation of the ruthenium complex by 796 nm irradiation instead of the traditional 969 nm irradiation, without loss of efficiency. The use of 796 nm light circumvents the main disadvantage associated with high-intensity 969 nm light, i.e., heating. Meanwhile, ruthenium complexes form a stable, polar coating for UCNPs, which improves their dispersibility and colloidal stability in aqueous media. Overall, although CSS-UCNPs appear to be a useful platform for photoactivation of the ruthenium polypyridyl complexes using light in the first phototherapeutic window, 50 W·cm^{-2} is too high for phototherapeutic applications. From our work, we can name three alternative design principles that would allow for solving this issue. First, the bidentate thioether ligand may be modified into a monodentate ligand, to avoid the need for activating two photosubstitution reactions.[10] Secondly, Er^{3+}-doped UCNPs emitting in the green region of the spectrum may be preferred over blue Tm^{3+}-doped UCNPs because three-photon upconversion is inherently brighter at low power densities than four-photon upconversion. Such modifications will require the ruthenium complex to also have its absorption maximum shifted into the green area of the spectrum, to keep optimal spectral overlap. Finally, new CSS nanomaterials with improved upconversion efficiencies are needed that maximize the upconverted light intensity without H_2O quenching. When these design principles are combined, ruthenium-UCNP nanoconjugates may become relevant for phototherapy provided significant amounts of ruthenium complexes are released within shorter (≤1 h) NIR irradiation times, and this occurs at an excitation power density that remains lower than the maximum permissible exposure for skin allowed by the American National Standard for Safe Use of Lasers, i.e., 0.726 W·cm^{-2}.[34,64,65]

ASSOCIATED CONTENT

Supporting Information

The Supporting Information is available free of charge at https://pubs.acs.org/doi/10.1021/acs.inorgchem.0c00043.

https://dx.doi.org/10.1021/acs.inorgchem.0c00043
Inorg. Chem. 2020, 59, 14807−14818

Details of the ligand synthesis, ruthenium complex synthesis, UCNP synthesis, and nanoparticle surface ligand exchange, details and spectra of nanoparticle characterization by XRD, TGA, TEM, ICP-OES, DLS, and ζ-potential measurements, spectroscopic details for quantum-yield measurements (for photosubstitution, singlet oxygen generation, and phosphorescence), upconversion luminescence, and photosubstitution experiments, dark stability measurements, and NMR spectra (PDF)

AUTHOR INFORMATION

Corresponding Authors

Marta M. Natile − *Institute of Condensed Matter Chemistry and Technologies for Energy, National Research Council (CNR), Department of Chemical Sciences, University of Padova, 35131 Padova, Italy;* orcid.org/0000-0001-5591-2670; Email: martamaria.natile@unipd.it

Sylvestre Bonnet − *Leiden Institute of Chemistry, Leiden University, 2300 RA Leiden, The Netherlands;* orcid.org/0000-0002-5810-3657; Email: bonnet@chem.leidenuniv.nl

Author

Michael S. Meijer − *Leiden Institute of Chemistry, Leiden University, 2300 RA Leiden, The Netherlands;* orcid.org/0000-0003-0877-2374

Complete contact information is available at: https://pubs.acs.org/10.1021/acs.inorgchem.0c00043

Notes

The authors declare no competing financial interest.

ACKNOWLEDGMENTS

The COST action CM1403 ("The European Upconversion Network") is thanked for stimulating scientific discussion and for granting two short-term scientific missions to M.S.M. The COST Action CA 17140 "Cancer Nanomedicine from the Bench to the Bedside" is thanked for stimulating scientific discussion. The European Research Council is acknowledged for a starting grant to S.B. The Holland Research School for Molecular Chemistry is thanked for a fellowship to M.M.N. The National Research Council (Italy, CNR) is thanked for an STM fellowship to M.M.N. Dr. F. Boldrin and Dr. F. Caicci (Department of Biology, University of Padova) are thanked for producing TEM images. F. Natile is kindly acknowledged for support in the table of contents graphic design. S.B. and M.S.M. kindly acknowledge Prof. E. Bouwman (Leiden University) for scientific discussion and support. M.M.N. kindly acknowledges Prof. L. Armelao (University of Padova) for scientific support.

REFERENCES

(1) Velema, W. A.; Szymanski, W.; Feringa, B. L. Photopharmacology: Beyond Proof of Principle. *J. Am. Chem. Soc.* **2014**, *136*, 2178−2191.

(2) Bonnet, S. Why Develop Photoactivated Chemotherapy? *Dalton Transactions* **2018**, *47*, 10330−10343.

(3) Farrer, N. J.; Salassa, L.; Sadler, P. J. Photoactivated Chemotherapy (PACT): the Potential of Excited-State D-block Metals in Medicine. *Dalton Transactions* **2009**, *38*, 10690−10701.

(4) Garner, R. N.; Gallucci, J. C.; Dunbar, K. R.; Turro, C. [Ru(bpy)2(5-cyanouracil)2]2+ as a Potential Light-Activated Dual-Action Therapeutic Agent. *Inorg. Chem.* **2011**, *50*, 9213−9215.

(5) Zayat, L.; Calero, C.; Alborés, P.; Baraldo, L.; Etchenique, R. A New Strategy for Neurochemical Photodelivery: Metal−Ligand Heterolytic Cleavage. *J. Am. Chem. Soc.* **2003**, *125*, 882−883.

(6) Shi, G.; Monro, S.; Hennigar, R.; Colpitts, J.; Fong, J.; Kasimova, K.; Yin, H.; DeCoste, R.; Spencer, C.; Chamberlain, L.; Mandel, A.; Lilge, L.; McFarland, S. A. Ru(II) Dyads Derived from α-oligothiophenes: A New Class of Potent and Versatile Photosensitizers for PDT. *Coord. Chem. Rev.* **2015**, *282*−*283*, 127−138.

(7) Hess, J.; Huang, H.; Kaiser, A.; Pierroz, V.; Blacque, O.; Chao, H.; Gasser, G. Evaluation of the Medicinal Potential of Two Ruthenium(II) Polypyridine Complexes as One- and Two-Photon Photodynamic Therapy Photosensitizers. *Chem. - Eur. J.* **2017**, *23*, 9888−9896.

(8) Hidayatullah, A. N.; Wachter, E.; Heidary, D. K.; Parkin, S.; Glazer, E. C. Photoactive Ru(II) Complexes With Dioxinophenanthroline Ligands Are Potent Cytotoxic Agents. *Inorg. Chem.* **2014**, *53*, 10030−10032.

(9) Karaoun, N.; Renfrew, A. K. A Luminescent Ruthenium(II) Complex for Light-Triggered Drug Release and Live Cell Imaging. *Chem. Commun.* **2015**, *51*, 14038−14041.

(10) Lameijer, L. N.; Ernst, D.; Hopkins, S. L.; Meijer, M. S.; Askes, S. H. C.; Le Dévédec, S. E.; Bonnet, S. A Red Light-Activated Ruthenium-Caged NAMPT Inhibitor Remains Phototoxic in Hypoxic Cancer Cells. *Angew. Chem., Int. Ed.* **2017**, *56*, 11549−11553.

(11) Hopkins, S. L.; Siewert, B.; Askes, S. H. C.; Veldhuizen, P.; Zwier, R.; Heger, M.; Bonnet, S. An In Vitro Cell Irradiation Protocol for Testing Photopharmaceuticals and the Effect of Blue, Green, and Red Light on Human Cancer Cell Lines. *Photochemical & Photobiological Sciences* **2016**, *15*, 644−653.

(12) Vogel, A.; Venugopalan, V. Mechanisms of Pulsed Laser Ablation of Biological Tissues. *Chem. Rev.* **2003**, *103*, 577−644.

(13) Sun, W.; Wen, Y.; Thiramanas, R.; Chen, M.; Han, J.; Gong, N.; Wagner, M.; Jiang, S.; Meijer, M. S.; Bonnet, S.; Butt, H.-J.; Mailänder, V.; Liang, X.-J.; Wu, S. Red-Light-Controlled Release of Drug−Ru Complex Conjugates from Metallopolymer Micelles for Phototherapy in Hypoxic Tumor Environments. *Adv. Funct. Mater.* **2018**, *28*, 1804227.

(14) Loftus, L. M.; Al-Afyouni, K. F.; Turro, C. New Ru(II) Scaffold for Photoinduced Ligand Release with Red Light in the Photodynamic Therapy (PDT) Window. *Chem. - Eur. J.* **2018**, *24*, 11550−11553.

(15) Askes, S. H. C.; Bahreman, A.; Bonnet, S. Activation of a Photodissociative Ruthenium Complex by Triplet−Triplet Annihilation Upconversion in Liposomes. *Angew. Chem., Int. Ed.* **2014**, *53*, 1029−1033.

(16) Huang, L.; Zhao, Y.; Zhang, H.; Huang, K.; Yang, J.; Han, G. Expanding Anti-Stokes Shifting in Triplet−Triplet Annihilation Upconversion for In Vivo Anticancer Prodrug Activation. *Angew. Chem., Int. Ed.* **2017**, *56*, 14400−14404.

(17) Perfahl, S.; Natile, M. M.; Mohamad, H. S.; Helm, C. A.; Schulzke, C.; Natile, G.; Bednarski, P. J. Photoactivation of Diiodido−Pt(IV) Complexes Coupled to Upconverting Nanoparticles. *Mol. Pharmaceutics* **2016**, *13*, 2346−2362.

(18) Gorris, H. H.; Resch-Genger, U. Perspectives and Challenges of Photon-Upconversion Nanoparticles − Part II Bioanalytical Applications. *Anal. Bioanal. Chem.* **2017**, *409*, 5875−5890.

(19) Li, X.; Zhang, F.; Zhao, D. Lab on Upconversion Nanoparticles: Optical Properties and Applications Engineering via Designed Nanostructure. *Chem. Soc. Rev.* **2015**, *44*, 1346−1378.

(20) Näreoja, T.; Deguchi, T.; Christ, S.; Peltomaa, R.; Prabhakar, N.; Fazeli, E.; Perälä, N.; Rosenholm, J. M.; Arppe, R.; Soukka, T.; Schäferling, M. Ratiometric Sensing and Imaging of Intracellular pH Using Polyethylenimine-Coated Photon Upconversion Nanoprobes. *Anal. Chem.* **2017**, *89*, 1501−1508.

(21) Drees, C.; Raj, A. N.; Kurre, R.; Busch, K. B.; Haase, M.; Piehler, J. Engineered Upconversion Nanoparticles for Resolving Protein Interactions inside Living Cells. *Angew. Chem., Int. Ed.* **2016**, *55*, 11668−11672.

https://dx.doi.org/10.1021/acs.inorgchem.0c00043
Inorg. Chem. 2020, 59, 14807−14818

(22) Bagheri, A.; Arandiyan, H.; Boyer, C.; Lim, M. Lanthanide-Doped Upconversion Nanoparticles: Emerging Intelligent Light-Activated Drug Delivery Systems. *Advanced Science* **2016**, *3*, 1500437.
(23) Deng, K.; Li, C.; Huang, S.; Xing, B.; Jin, D.; Zeng, Q.; Hou, Z.; Lin, J. Recent Progress in Near Infrared Light Triggered Photodynamic Therapy. *Small* **2017**, *13*, 1702299.
(24) Wang, D.; Xue, B.; Kong, X.; Tu, L.; Liu, X.; Zhang, Y.; Chang, Y.; Luo, Y.; Zhao, H.; Zhang, H. 808 nm Driven Nd^{3+}-Sensitized Upconversion Nanostructures for Photodynamic Therapy and Simultaneous Fluorescence Imaging. *Nanoscale* **2015**, *7*, 190−197.
(25) Chen, Z.; Thiramanas, R.; Schwendy, M.; Xie, C.; Parekh, S. H.; Mailänder, V.; Wu, S. Upconversion Nanocarriers Encapsulated with Photoactivatable Ru Complexes for Near-Infrared Light-Regulated Enzyme Activity. *Small* **2017**, *13*, 1700997.
(26) Chen, W.; Shi, C.; Tao, T.; Ji, M.; Zheng, S.; Sang, X.; Liu, X.; Qiu, J. Optical Temperature Sensing with Minimized Heating Effect using Core-Shell Upconversion Nanoparticles. *RSC Adv.* **2016**, *6*, 21540−21545.
(27) Sedlmeier, A.; Achatz, D. E.; Fischer, L. H.; Gorris, H. H.; Wolfbeis, O. S. Photon Upconverting Nanoparticles for Luminescent Sensing of Temperature. *Nanoscale* **2012**, *4*, 7090−7096.
(28) Vetrone, F.; Naccache, R.; Zamarrón, A.; Juarranz de la Fuente, A.; Sanz-Rodríguez, F.; Martinez Maestro, L.; Martín Rodriguez, E.; Jaque, D.; García Solé, J.; Capobianco, J. A. Temperature Sensing Using Fluorescent Nanothermometers. *ACS Nano* **2010**, *4*, 3254−3258.
(29) Liu, X.; Chen, H.-C.; Kong, X.; Zhang, Y.; Tu, L.; Chang, Y.; Wu, F.; Wang, T.; Reek, J. N. H.; Brouwer, A. M.; Zhang, H. Near Infrared Light-Driven Water Oxidation in a Molecule-Based Artificial Photosynthetic Device using an Upconversion Nano-Photosensitizer. *Chem. Commun.* **2015**, *51*, 13008−13011.
(30) Tang, Y.; Di, W.; Zhai, X.; Yang, R.; Qin, W. NIR-Responsive Photocatalytic Activity and Mechanism of $NaYF_4$:Yb,Tm@TiO_2 Core−Shell Nanoparticles. *ACS Catal.* **2013**, *3*, 405−412.
(31) Hofmann, C. L. M.; Eriksen, E. H.; Fischer, S.; Richards, B. S.; Balling, P.; Goldschmidt, J. C. Enhanced Upconversion in One-Dimensional Photonic Crystals: a Simulation-Based Assessment Within Realistic Material and Fabrication Constraints. *Opt. Express* **2018**, *26*, 7537−7554.
(32) Kim, W. J.; Nyk, M.; Prasad, P. N. Color-coded Multilayer Photopatterned Microstructures using Lanthanide(III) Ion Co-Doped $NaYF_4$ Nanoparticles with Upconversion Luminescence for Possible Applications in Security. *Nanotechnology* **2009**, *20*, 185301.
(33) Chen, G.; Qiu, H.; Prasad, P. N.; Chen, X. Upconversion Nanoparticles: Design, Nanochemistry, and Applications in Theranostics. *Chem. Rev.* **2014**, *114*, 5161−5214.
(34) Chen, Z.; Sun, W.; Butt, H.-J.; Wu, S. Upconverting-Nanoparticle-Assisted Photochemistry Induced by Low-Intensity Near-Infrared Light: How Low Can We Go? *Chem. - Eur. J.* **2015**, *21*, 9165−9170.
(35) Wang, Y.-F.; Liu, G.-Y.; Sun, L.-D.; Xiao, J.-W.; Zhou, J.-C.; Yan, C.-H. Nd^{3+}-Sensitized Upconversion Nanophosphors: Efficient In Vivo Bioimaging Probes with Minimized Heating Effect. *ACS Nano* **2013**, *7*, 7200−7206.
(36) Xie, X.; Gao, N.; Deng, R.; Sun, Q.; Xu, Q.-H.; Liu, X. Mechanistic Investigation of Photon Upconversion in Nd^{3+}-Sensitized Core−Shell Nanoparticles. *J. Am. Chem. Soc.* **2013**, *135*, 12608−12611.
(37) Zhong, Y.; Tian, G.; Gu, Z.; Yang, Y.; Gu, L.; Zhao, Y.; Ma, Y.; Yao, J. Elimination of Photon Quenching by a Transition Layer to Fabricate a Quenching-Shield Sandwich Structure for 800 nm Excited Upconversion Luminescence of Nd^{3+}-Sensitized Nanoparticles. *Adv. Mater.* **2014**, *26*, 2831−2837.
(38) Shen, J.; Chen, G.; Vu, A.-M.; Fan, W.; Bilsel, O. S.; Chang, C.-C.; Han, G. Engineering the Upconversion Nanoparticle Excitation Wavelength: Cascade Sensitization of Tri-doped Upconversion Colloidal Nanoparticles at 800 nm. *Adv. Opt. Mater.* **2013**, *1*, 644−650.
(39) Würth, C.; Fischer, S.; Grauel, B.; Alivisatos, A. P.; Resch-Genger, U. Quantum Yields, Surface Quenching and Passivation Efficiency for Ultra-Small Core/Shell Upconverting Nanoparticles. *J. Am. Chem. Soc.* **2018**, *140*, 4922−4928.
(40) Johnson, N. J. J.; Korinek, A.; Dong, C.; van Veggel, F. C. J. M. Self-Focusing by Ostwald Ripening: A Strategy for Layer-by-Layer Epitaxial Growth on Upconverting Nanocrystals. *J. Am. Chem. Soc.* **2012**, *134*, 11068−11071.
(41) Johnson, N. J. J.; van Veggel, F. C. J. M. Lanthanide-Based Heteroepitaxial Core−Shell Nanostructures: Compressive versus Tensile Strain Asymmetry. *ACS Nano* **2014**, *8*, 10517−10527.
(42) Ruggiero, E.; Habtemariam, A.; Yate, L.; Mareque-Rivas, J. C.; Salassa, L. Near Infrared Photolysis of a Ru Polypyridyl Complex by Upconverting Nanoparticles. *Chem. Commun.* **2014**, *50*, 1715−1718.
(43) Shi, H.; Fang, T.; Tian, Y.; Huang, H.; Liu, Y. A Dual-Fluorescent Nano-Carrier for Delivering Photoactive Ruthenium Polypyridyl Complexes. *J. Mater. Chem. B* **2016**, *4*, 4746−4753.
(44) Ellahioui, Y.; Patra, M.; Mari, C.; Kaabi, R.; Karges, J.; Gasser, G.; Gómez-Ruiz, S. Mesoporous Silica Nanoparticles Functionalised with a Photoactive Ruthenium(II) Complex: Exploring the Formulation of a Metal-Based Photodynamic Therapy Photosensitiser. *Dalton Transactions* **2019**, *48*, 5940−5951.
(45) Zhang, Y.; Yu, Z.; Li, J.; Ao, Y.; Xue, J.; Zeng, Z.; Yang, X.; Tan, T. T. Y. Ultrasmall-Superbright Neodymium-Upconversion Nanoparticles via Energy Migration Manipulation and Lattice Modification: 808 nm-Activated Drug Release. *ACS Nano* **2017**, *11*, 2846−2857.
(46) Xiang, H.-J.; Deng, Q.; An, L.; Guo, M.; Yang, S.-P.; Liu, J.-G. Tumor Cell Specific and Lysosome-Targeted Delivery of Nitric Oxide for Enhanced Photodynamic Therapy Triggered by 808 nm Near-Infrared Light. *Chem. Commun.* **2016**, *52*, 148−151.
(47) Ding, Y.; Wu, F.; Zhang, Y.; Liu, X.; de Jong, E. M. L. D.; Gregorkiewicz, T.; Hong, X.; Liu, Y.; Aalders, M. C. G.; Buma, W. J.; Zhang, H. Interplay between Static and Dynamic Energy Transfer in Biofunctional Upconversion Nanoplatforms. *J. Phys. Chem. Lett.* **2015**, *6*, 2518−2523.
(48) Wilhelm, S.; Kaiser, M.; Würth, C.; Heiland, J.; Carrillo-Carrion, C.; Muhr, V.; Wolfbeis, O. S.; Parak, W. J.; Resch-Genger, U.; Hirsch, T. Water Dispersible Upconverting Nanoparticles: Effects of Surface Modification on their Luminescence and Colloidal Stability. *Nanoscale* **2015**, *7*, 1403−1410.
(49) Sedlmeier, A.; Gorris, H. H. Surface Modification and Characterization of Photon-Upconverting Nanoparticles for Bioanalytical Applications. *Chem. Soc. Rev.* **2015**, *44*, 1526−1560.
(50) Cao, P.; Tong, L.; Hou, Y.; Zhao, G.; Guerin, G.; Winnik, M. A.; Nitz, M. Improving Lanthanide Nanocrystal Colloidal Stability in Competitive Aqueous Buffer Solutions using Multivalent PEG-Phosphonate Ligands. *Langmuir* **2012**, *28*, 12861−12870.
(51) Zhao, G.; Tong, L.; Cao, P.; Nitz, M.; Winnik, M. A. Functional PEG−PAMAM-Tetraphosphonate Capped $NaLnF_4$ Nanoparticles and their Colloidal Stability in Phosphate Buffer. *Langmuir* **2014**, *30*, 6980−6989.
(52) Collin, J.-P.; Jouvenot, D.; Koizumi, M.; Sauvage, J.-P. $Ru(phen)_2(bis\text{-}thioether)^{2+}$ complexes: Synthesis and Photosubstitution Reactions. *Inorg. Chim. Acta* **2007**, *360*, 923−930.
(53) Garner, R. N.; Joyce, L. E.; Turro, C. Effect of Electronic Structure on the Photoinduced Ligand Exchange of Ru(II) Polypyridine Complexes. *Inorg. Chem.* **2011**, *50*, 4384−4391.
(54) Meijer, M. S.; Talens, V. S.; Hilbers, M. F.; Kieltyka, R. E.; Brouwer, A. M.; Natile, M. M.; Bonnet, S. NIR-Light-Driven Generation of Reactive Oxygen Species Using Ru(II)-Decorated Lipid-Encapsulated Upconverting Nanoparticles. *Langmuir* **2019**, *35*, 12079−12090.
(55) Wang, F.; Wang, J.; Liu, X. Direct Evidence of a Surface Quenching Effect on Size-Dependent Luminescence of Upconversion Nanoparticles. *Angew. Chem., Int. Ed.* **2010**, *49*, 7456−7460.
(56) Meijer, M. S.; Bonnet, S. Diastereoselective Synthesis and Two-Step Photocleavage of Ruthenium Polypyridyl Complexes Bearing a Bis(thioether) Ligand. *Inorg. Chem.* **2019**, *58*, 11689−11698.

https://dx.doi.org/10.1021/acs.inorgchem.0c00043
Inorg. Chem. 2020, 59, 14807−14818

(57) Snellenburg, J. J.; Laptenok, S.; Seger, R.; Mullen, K. M.; van Stokkum, I. H. M. Glotaran: A Java-Based Graphical User Interface for the R Package TIMP. *Journal of Statistical Software* **2012**, *49*, 22.
(58) Dong, A.; Ye, X.; Chen, J.; Kang, Y.; Gordon, T.; Kikkawa, J. M.; Murray, C. B. A Generalized Ligand-Exchange Strategy Enabling Sequential Surface Functionalization of Colloidal Nanocrystals. *J. Am. Chem. Soc.* **2011**, *133*, 998−1006.
(59) Kowalik, P.; Elbaum, D.; Mikulski, J.; Fronc, K.; Kamińska, I.; Morais, P. C.; Eduardo de Souza, P.; Nunes, R. B.; Veiga-Souza, F. H.; Gruzeł, G.; Minikayev, R.; Wojciechowski, T.; Mosiniewicz-Szablewska, E.; Szewczyk, M.; Pawlyta, M.; Sienkiewicz, A.; Łapiński, M.; Zajdel, K.; Stępień, P.; Szczepkowski, J.; Jastrzębski, W.; Frontczak-Baniewicz, M.; Paszkowicz, W.; Sikora, B. Upconversion Fluorescence Imaging of HeLa Cells using ROS Generating SiO_2-coated Lanthanide-Doped $NaYF_4$ Nanoconstructs. *RSC Adv.* **2017**, *7*, 30262−30273.
(60) Good, N. E.; Winget, G. D.; Winter, W.; Connolly, T. N.; Izawa, S.; Singh, R. M. M. Hydrogen Ion Buffers for Biological Research. *Biochemistry* **1966**, *5*, 467−477.
(61) Plohl, O.; Kraft, M.; Kovač, J.; Belec, B.; Ponikvar-Svet, M.; Würth, C.; Lisjak, D.; Resch-Genger, U. Optically Detected Degradation of $NaYF_4$:Yb,Tm-Based Upconversion Nanoparticles in Phosphate Buffered Saline Solution. *Langmuir* **2017**, *33*, 553−560.
(62) Ruggiero, E.; Garino, C.; Mareque-Rivas, J. C.; Habtemariam, A.; Salassa, L. Upconverting Nanoparticles Prompt Remote Near-Infrared Photoactivation of Ru(II)−Arene Complexes. *Chem. - Eur. J.* **2016**, *22*, 2801−2811.
(63) Tong, L.; Lu, E.; Pichaandi, J.; Cao, P.; Nitz, M.; Winnik, M. A. Quantification of Surface Ligands on $NaYF_4$ Nanoparticles by Three Independent Analytical Techniques. *Chem. Mater.* **2015**, *27*, 4899−4910.
(64) Ziegelberger, G. ICNIRP guidelines on limits of exposure to incoherent visible and infrared radiation. *Health Phys.* **2013**, *105*, 74−96.
(65) *American National Standard for Safe Use of Lasers*; Laser Institute of America: Orlando, FL, 2007; pp 1−249.

https://dx.doi.org/10.1021/acs.inorgchem.0c00043
Inorg. Chem. 2020, 59, 14807−14818